Optik 124 (2013) 5218–5224

Contents lists available at ScienceDirect

Optik

journal homepage: www.elsevier.de/ijleo

An FDTD based numerical analysis of microwave propagation properties in a skin–fat tissue layers

H.Z. Alisoy[a,*], S. Barlaz Us[b], B.B. Alagoz[a]

[a] Inonu University Faculty of Engineering, Department of Electric–Electronic Engineering, Turkey
[b] Inonu University Faculty of Medicine, Department of Radiation Oncology, Turkey

ARTICLE INFO

Article history:
Received 15 October 2012
Accepted 15 March 2013

Keywords:
Microwave propagation in biological tissue
FDTD method
SAR distribution

ABSTRACT

This study theoretically investigates wave propagation properties at the interface of air–skin–fat tissues for a microwave frequency of 6.8 GHz. For this proposes, propagation of the microwaves in a biological tissue model of skin–fat are numerically analyzed by using FDTD method for the transverse magnetic (TM) mode of 2D-Maxwell's equations. These analyses are conducted for various point source placements such as none-contacting, embedded to skin and embedded to fat configurations. Electric field intensity and SAR distribution across the air–skin–fat tissue layers are revealed. The energy penetration and absorption degrees of planar skin–fat tissue layers are discussed in a physical origin. The large electrical impedance mismatches between the tissue layers result in reflection of microwaves from the interface of layers. Skin layer exhibits a considerable wave reflection property due to the high reflection coefficient at air–skin and skin–fat interfaces.

1. Introduction

Advance in microwave based medical technology requires comprehension of electromagnetic wave (EMW) propagation within the biological tissues. The EMW propagation simulation on tissue models has a substantial role in not only research activities but also estimating the possible effects of clinical treatments based on the microwave technology (MT).

Regional microwave energy absorption by the biological tissue results in heating the region [1]. One of applications of electromagnetic field in medical treatment is hyperthermia [2–4]. Clinical hyperthermia is used to reduce or eliminate tumors by means of controlled heating. Obtaining reliable and uniform heating at deep tissue sites is one of main concerns in applicator design for clinical hyperthermia applications. Interaction and propagation of EM waves in tissue layers should be known to estimate possible effects of applicators.

Finite difference time domain method, which is shortly abbreviated as FDTD in the literature, is based on the solving Maxwell equations in a spatio-temporal domain directly according to the finite differences method. FDTD has become a versatile numerical analysis tool which has been used nearly for the solution of many electromagnetic problems since its first declaration in 1966 [5–12]. The studies of the interaction of electromagnetic waves (EMW) with the biological tissues date back to the beginning of 1950s. Gabriel et al. published a literature survey for the dielectric features of biological tissues and presented them graphically [13]. They showed the conductivity and dielectric constants for several organs and tissues for various frequency intervals and establish a basic literature. Afterward, many approaches were proposed for the numerical analysis of the distribution of electromagnetic waves in a tissue [5–7]. Drezek et al. combined FDTD and pulse reply technique in order to calculate the light spreading feature of biological tissues [8]. Bérenger introduced the Hygens subgridding technique for a finer spatial sampling of lossy media in FDTD method [9]. Costen et al. were examined the validity of the Hygens subgridding technique in the first order Debye media such as the anatomical structures [14]. Many numerical studies analyzing impacts of wireless transmitter devices at GHz frequency range on human body was done for a close antenna-body configurations [10,15,16].

In this study, electric field intensity and SAR (specific absorption rate) distributions are analyzed in order to investigate the interaction of microwave at 6.8 GHz by the planar skin–fat layer. For this proposes, a 2D microwave propagation simulation based on FDTD method for the transverse magnetic (TM) mode is used to demonstrate impacts of multi-layer tissues on electric field intensity distribution and SAR distribution across a planar cross-section of the 3D tissue model in Fig. 1(a). This reduces the computational complexity of simulation due to inhomogeneity of planer layers media appears on this cross-section. Electrical parameters of skin–fat tissue model used were estimated from electrical characterization of anatomical tissues reported by Costen et al. [14]. By

* Corresponding author.
E-mail address: hafiz.alisoy@inonu.edu.tr (H.Z. Alisoy).

0030-4026/$ – see front matter © 2013 Elsevier GmbH. All rights reserved.
http://dx.doi.org/10.1016/j.ijleo.2013.03.085

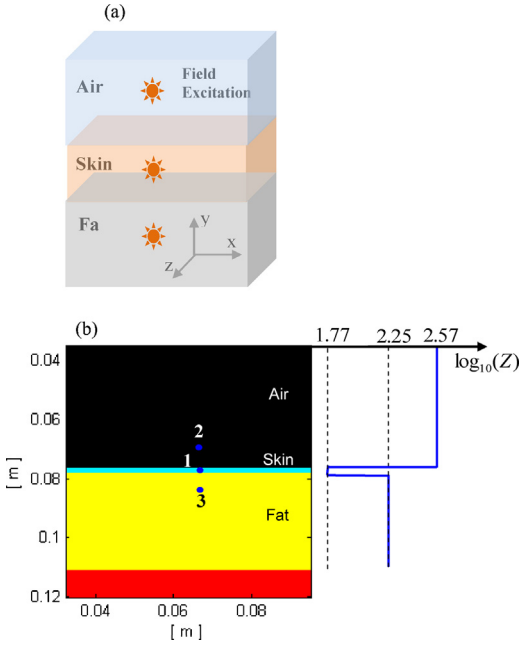

Fig. 1. (a) 3D representation of a skin–fat–muscle tissue layers. (b) Skin–fat–muscle simulation model for point sources configuration (embedded into the skin (1), 10 mm above the skin (2) and 10 mm below the skin (3)) and on the right hand side, characteristic impedance distribution in logarithmic scale trough vertical axis (the skin layer has a thickness of 2 mm, the fat layer has a thickness of 33 mm and a muscle layer extents below the fat layer).

using the parameters of Costen et al., dielectric constant parameters of skin–fat–muscle layers were calculated according to Debye model and effective conductivity are calculated via the formula used by Lagendijk [2]. The tissue densities for SAR calculations were directly taken from values reported by Chapla et al. [17]. Numerical analysis of EM wave absorption of the tissue layers were managed in two tasks: firstly, EM wave propagation simulation were conducted by the model parameters of air–skin–fat, and then SAR distribution was calculated by using the electric field intensity distribution obtained in the first task. Those analyses were conducted for the various configurations of point applicator, which are none-contacting antenna, a contact point antenna embedded to skin layer and a contact point antenna embedded below the skin layer. In the light of simulation results, basic physical mechanisms having effect on SAR distribution are discussed for a multilayer lossy media such as biological tissues.

2. Methodology

2.1. FDTD based numerical simulation of electromagnetic wave propagation in a lossy inhomogeneous media

Real wave propagation mediums exhibit attenuation effects, which is mainly characterized by a loss term, namely conductivity. In order to model EM propagation in the lossy mediums, Maxwell equations was written as the following [13]:

$$\varepsilon\frac{\partial\vec{E}}{\partial t} = \nabla\times\vec{H} - \sigma\vec{E} \tag{1}$$

$$\frac{\partial\vec{H}}{\partial t} = -\frac{1}{\mu_0}\nabla\times\vec{E} \tag{2}$$

Here, the parameter σ represents the conductivity. One can reorganize time dependence of electric field in Eq. (1) as,

$$\frac{\partial\vec{E}}{\partial t} = \frac{1}{\varepsilon_r\varepsilon_0}\nabla\times\vec{H} - \frac{\sigma}{\varepsilon_r\varepsilon_0}\vec{E} \tag{3}$$

if $\tilde{E} = \vec{E}\sqrt{(\varepsilon_0/\mu_0)}$ normalization is made for the electric field vector and the wave propagation in transverse magnetic (TM) mode is written for a two-dimensional (2D) spatial domain, the following equations are written.

$$\frac{\partial\tilde{E}_z(t)}{\partial t} = \frac{1}{\varepsilon_r\sqrt{\varepsilon_0\mu_0}}\left(\frac{\partial H_y(t)}{\partial x} - \frac{\partial H_x(t)}{\partial y}\right) - \frac{\sigma}{\varepsilon_r\varepsilon_0}\tilde{E}_z(t) \tag{4}$$

$$\frac{\partial H_x(t)}{\partial t} = -\frac{1}{\sqrt{\varepsilon_0\mu_0}}\frac{\partial\tilde{E}_z(t)}{\partial y} \tag{5}$$

$$\frac{\partial H_y(t)}{\partial t} = \frac{1}{\sqrt{\varepsilon_0\mu_0}}\frac{\partial\tilde{E}_z(t)}{\partial x} \tag{6}$$

When finite differences linearization is applied to the derivatives terms in Eqs. (4)–(6), the following finite difference equations are obtained:

$$H_x^{n+1/2}(i,j) = H_x^{n-1/2}(i,j) - \frac{\Delta t}{\sqrt{\varepsilon_0\mu_0}}\frac{\tilde{E}_z^n(i,j+1) - \tilde{E}_z^n(i,j)}{\Delta y} \tag{7}$$

$$H_y^{n+1/2}(i,j) = H_y^{n-1/2}(i,j) + \frac{\Delta t}{\sqrt{\varepsilon_0\mu_0}}\frac{\tilde{E}_z^n(i+1,j) - \tilde{E}_z^n(i,j)}{\Delta x} \tag{8}$$

$$\tilde{E}_z^{n+1}(i,j) = \tilde{E}_z^n(i,j) - \frac{\Delta t}{\varepsilon_r\sqrt{\varepsilon_0\mu_0}}\left(\frac{H_x^{n+1/2}(i,j) - H_x^{n+1/2}(i,j-1)}{\Delta y} - \frac{H_y^{n+1/2}(i,j) - H_y^{n+1/2}(i-1,j)}{\Delta x}\right) - \frac{\sigma\Delta t}{\varepsilon_r\varepsilon_0}\frac{\tilde{E}_z^{n+1}(i,j) + \tilde{E}_z^n(i,j)}{2} \tag{9}$$

The parameters Δx and Δy are horizontal and vertical unit distances for 2D spatial domain. A square solution point grid on this 2D plane was defined in the simulation by setting $\Delta x = \Delta y$. The parameter Δt is a unit time increment for the solutions in temporal domain. In order to obtain a stable EM wave propagation in the spatio-temporal domain, the Courant stability criteria, expressed as $\Delta t \le (\Delta x/(\sqrt{2}\cdot c))$, was considered to determine an appropriate value of Δt. Here, $c = 1/\sqrt{\varepsilon_0\mu_0}$ stands for the velocity of electromagnetic wave in a vacuum. By taking into account the unit time increment as $\Delta t = (\Delta x/(\sqrt{2}\cdot c))$ for a stable wave propagation on a 2D square solution grid, Eq. (9) can be rearranged as the following [18,19],

$$\tilde{E}_z^{n+1}(i,j) = \frac{(1-\alpha)}{(1+\alpha)}\tilde{E}_z^n(i,j) - \frac{1/\sqrt{2}}{\varepsilon_r(1+\alpha)}[H_x^{n+1/2}(i,j) - H_x^{n+1/2}(i,j-1) + H_y^{n+1/2}(i-1,j) - H_y^{n+1/2}(i,j)], \quad \text{where} \quad \alpha = \frac{\Delta t\cdot\sigma}{2\varepsilon_r\varepsilon_0}. \tag{10}$$

The finite difference equations given by Eqs. (7), (8) and (10) were used to simulate microwave propagation in a lossy inhomogeneous media that was modeled by the electrical parameters, the dielectric constant and the conductivity. In simulations, excitation of electric field intensity was done according to hard source model that directly drives the field intensity via a relevant waveform function [20]. We used a sinusoidal waveform for the field excitation at 6.8 GHz in the simulations. Our simulations take about 12 min in average via Matlab Technical Programming platform running on a personnel computer (PC).

Table 1
The parameters of biological tissues at 6.8 GHz [14].

Medium	σ (S/m)	ε_∞	ε_s	τ_0 (ps)
Air	10^{-14}	1	1	0
Skin	0.49	30	79	62
Fat	3×10^{-2}	3.5	6.2	39
Muscle	0.7	42	100	49

2.2. Parametric modeling of skin–fat tissue model

A point source of 6.8 GHz sinusoid microwave has been used in the FDTD simulation. Values of electrical parameters (σ: conductivity, ε_s: static dielectric constant, ε_∞: optical dielectric constant and τ_0: relaxation time) to be used to estimate model parameters of skin–fat–muscle layers for 6.8 GHz microwaves are listed in Table 1.

The four parameters, listed in Table 1, applied to well-known Debye model and the measurable electric constant to be used in electrically modeling of the skin–fat tissue layers was calculated by the following formula [21],

$$\varepsilon_r = Re\left\{\varepsilon_\infty + \frac{\varepsilon_s-\varepsilon_\infty}{(1+j\varpi\tau_0)} - j\frac{\sigma}{\varepsilon_0\varpi}\right\} \tag{11}$$

ε_0 is the dielectric constant of vacuum and its value was taken 8854×10^{-12} F/m in the simulation. ω denotes the angular frequency and it is expressed as $\omega = 2\pi f$. Here, f is linear frequency value of EM wave.

By considering Table 1, the effective value of electrical conductivity to be used in the simulation was also calculated via the following formula [17],

$$\sigma_{eff} = \sigma - \omega\varepsilon_0 \quad imag\left\{\frac{\varepsilon_s-\varepsilon_\infty}{1+j\omega\tau_0}\right\} \tag{12}$$

SAR depends on the energy of EM waves, the conductance and the density parameters of the materials. In the simulations, SAR was calculated by the following formula [10,19,22,23].

$$\mathrm{SAR} = \sigma_{eff}\frac{|\vec{E}|^2}{2\rho} \tag{13}$$

where ρ (kg/m) and σ_{eff} (S/m) are the tissue density and the effective electrical conductivity, respectively.

The electrical parameters of skin–fat–muscle models used in the 2D FDTD simulation of microwave propagation at 6.8 GHz are listed in Table 2. In order to estimate SAR distribution of the skin–fat model by using Eq. (13), the electric field intensities are obtained from the 2D FDTD simulation and the tissue densities were taken from Table 2.

3. Simulation results and discussion

A microwave source at 6.8 GHz frequency placed to three different distances from the skin, marked by blue dots at (1)–(3) on the skin–fat–muscle test model represented in Fig. 1. In Fig. 1(b), each planar tissue layer was indicated with a color coding, where the black is for the air, the turquoise is for skin tissue, the yellow is for fat tissue and the red is for muscles tissue. The microwave point source indicated with blue color code. In simulations, a square grid with $\Delta y = \Delta x = 0.2$ mm unit distances was used to define discrete solution grid of electric field and magnetic field components. These unit distances provide a sufficient spatial sampling for 6.8 GHz EM wave propagation in the skin–fat tissues (a wavelength of 44 mm was solved with 220 point of the square solution grid). This excessive spatial sampling also provide an adequate spatial resolution to model the narrowest layer of the biological tissue, which is the skin layer with thickness of 2.0 mm. A time resolution of 0.47 ps ($\Delta t = 0.47$ ps) was used to comply with Courant stability criteria. In order to prevent boundary reflections from edges of simulation region, a boundary absorption region expanding with the same medium parameters of simulation region edges is used around the simulation region. Thus, the edge of simulation region behaved as an infinite medium for a limited simulation time period depending on the arrival time of reflected waves from the absorption region.

Table 2
The dielectric constant, electrical conductivity and tissue density values used in the numerical analysis of the skin–fat–muscle model at 6.8 GHz.

Medium	ε_r	σ_{eff} (S/m)	ρ (kg/m^3)
Air	1	10^{-14}	1.3
Skin	36.11	6.61	1118
Fat	4.21	0.48	999
Muscle	52.77	9.23	1119

Table 3
Reflection coefficients of the skin–fat–muscle simulation model.

Layers	R
Air to skin	−0.73
Skin to fat	0.50
Fat to muscle	−0.56

It would be better to give a brief discussion on impedance mismatches of layers and the resulting wave reflection phenomenon. As known, biophysical characteristics of tissues are determined by the conductivity, permittivity and permeability. Characteristic impedances of layers, defined as $Z = \sqrt{j\omega\mu/(\sigma+j\omega\varepsilon)}$, is an important parameter which determines reflection coefficient of interfaces between the layers. The characteristic impedance variation in the layers of the simulation model is illustrated in Fig. 1(b). Reflection coefficient (R) between the layers is calculated by,

$$R = \frac{Z_2 - Z_1}{Z_1 + Z_2}, \tag{14}$$

where Z_1 and Z_2 are characteristic impedances of the first and the second layer, respectively. The reflection coefficient takes value in the range of [−1,1], the value of one indicates the case of a full

Table 4
Some physical mechanisms effecting SAR distribution in a multilayer system with a with high reflection coefficients.

Effect	Region	Condition	Impact on SAR
Constructive reflection interference	Field close to layer interfaces	Appears when $R>0$	An increase in SAR level
Destructive reflection interference	Field close to layer interfaces	Appears when $R<0$	A decrease in SAR level
Conductance per mass density discrimination	On the layer interface	For sharp rise, $\frac{\sigma_{eff1}}{\rho_1}\cdot\left(\frac{\sigma_{eff2}}{\rho_2}\right)^{-1} \ll (1-\lvert R\rvert)$ For a sharp fall, $\frac{\sigma_{eff1}}{\rho_1}\cdot\left(\frac{\sigma_{eff2}}{\rho_2}\right)^{-1} \gg (1-\lvert R\rvert)$	Very sharp alteration of SAR level
EM attenuation (Beer–Lambert Law)	Interior of the layers	Large attenuation when $\alpha \gg 0$	Exponentially decaying SAR distribution inside layers

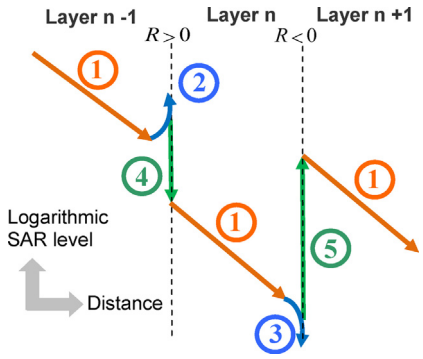

Fig. 2. A representation of physical mechanisms taking effect on peak SAR distribution in a multilayer media with high reflection coefficients and large conductance per mass density discrimination between layers.

reflection of waves from the interface between layers. A negative value of R indicates a 180° phase shift between reflected and incident waves. In Table 3, an estimation of the reflection coefficients for the layers of simulation model given in Fig. 1 is listed.

Sharp changes in characteristic impedances between layers results in a higher reflection coefficient and correspondingly a lower rate in wave transmission to next layers. This is main mechanism preventing a high EM energy penetration into the multi-layer mediums involving high impedance mismatches, because most of energy conveyed by EM wave reflected back from interface of tissue layers. Inside the layers, penetration of EM wave energy exponentially decays according to Beer–Lambert Law. An attenuation coefficient, expressed as $\alpha = -(1/r)\ln(|\vec{E}(r)|^2/|\vec{E}(0)|^2)$, is used to indicate degree of exponential decaying of EM wave intensity.

SAR distribution in a media depends on EM wave energy penetrated and material conductance per mass density regarding to Eq. (13). Table 4 categorizes some possible physical phenomena influencing SAR distribution in a multi-layer media with high reflection coefficients between layers. Fig. 2 illustrates changes in SAR distribution depending on these physical phenomena. Arrow 1 shows decreasing SAR level in layer due to EM attenuation (Beer–Lambert Law). Curved arrows 2 and 3 show effects of constructive and destructive reflection interferences on the SAR at the near field of layer interfaces. Sharp rises and fall patterns on the interface of layers (vertical arrows 4 and 5) represents changes in SAR distribution as a result of very large conductance per mass density discrimination.

In the case of a high positive reflection coefficient among to layers, a higher field intensity region occurs at the vicinity of one side of layer interfaces as a result of the constructive interference of incident and reflecting waves. This impact causes a slight rise in SAR distribution at the vicinity of layer interfaces. A high negative reflection coefficient leads to a destructive interference of reflected and incident waves, and hence results in a slight decreasing of SAR level at the vicinity of layers. Such reflection interference phenomenon is a factor causing altering SAR distribution at the one-side near field of interfaces of the biological tissue layers. An other factor resulting in very sharp variation of SAR levels at layer interfaces is the large differences in conductance per mass density, which is expressed by the rate of σ_{eff}/ρ. Sharply alterations in the rate of σ_{eff}/ρ in a multilayer system lead to sudden changes in SAR distribution on the interface of layers. These effects were clearly demonstrated in the simulation results presented in this section. In the previous studies, sudden increases and decreases on different tissue interfaces have been reported: Sullivan in [23] has reported a sudden SAR increases on the muscle–fat interface for the microwaves, and Moros et al. revealed a sudden power absorptions on the soft tissue–bone and soft tissue–lung interfaces for the ultrasound waves [24].

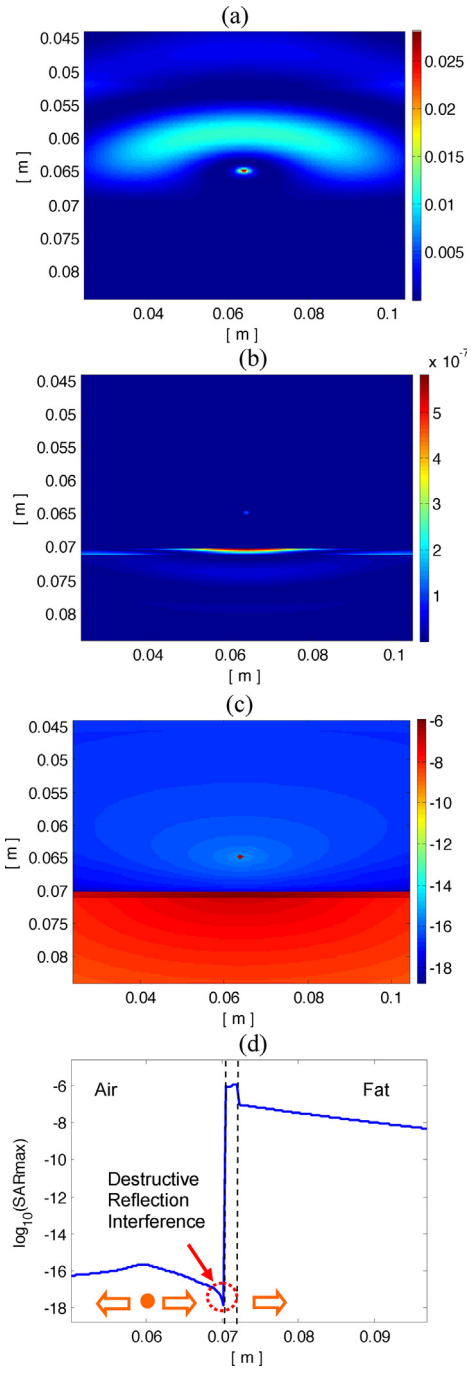

Fig. 3. A none-contacting point source is placed 10 mm above the skin. (a) Instant electric field intensity, (b) instant SAR distribution, (c) logarithmic peak SAR distribution and (d) logarithmic peak SAR distribution on vertical cross-section. The point indicates location of point antenna and arrows indicates direction of wave propagation though layer.

In the simulation results, the distribution of maximum SAR values (Peak SAR) recorded in simulation period is presented in addition to the mapping of instant electric field intensity and corresponding instant value of SAR distribution. The instant value of electric field intensity gives a snap-shot of EM propagation in the tissue model. This is important for temporal analysis of wave propagation among the tissue layers. The peak SAR distribution map reveals the tissue region where the maximal energy absorption was taken place.

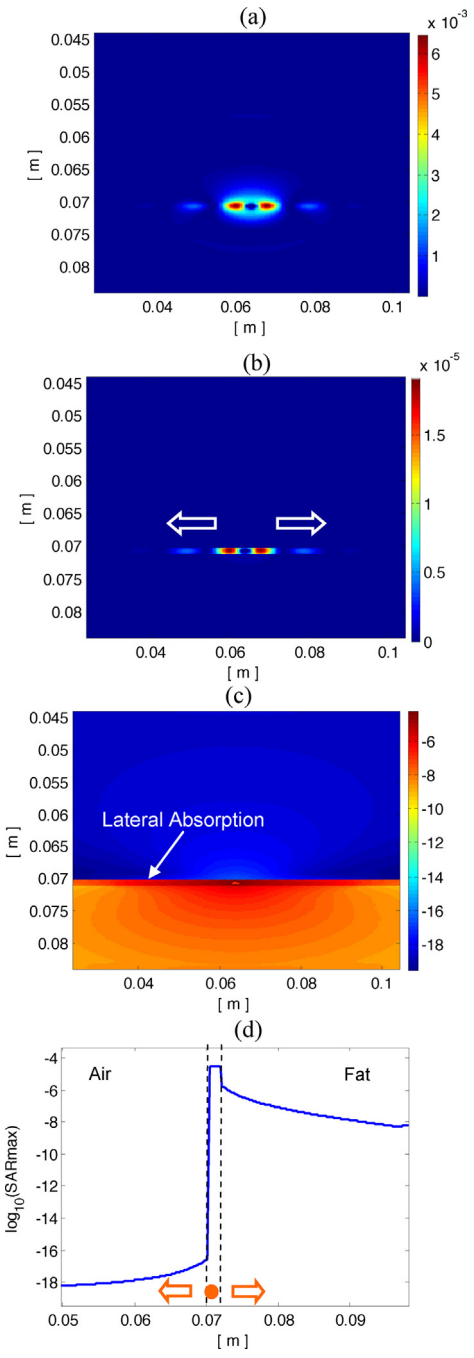

Fig. 4. A contact point source is embedded into the skin layer. (a) Instant electric field intensity, (b) instant SAR distribution, (c) logarithmic peak SAR distribution and (d) logarithmic peak SAR distribution on vertical cross-section. White arrows in (b) shows direction of EM wave propagation and the wave-guiding effect of skin layer.

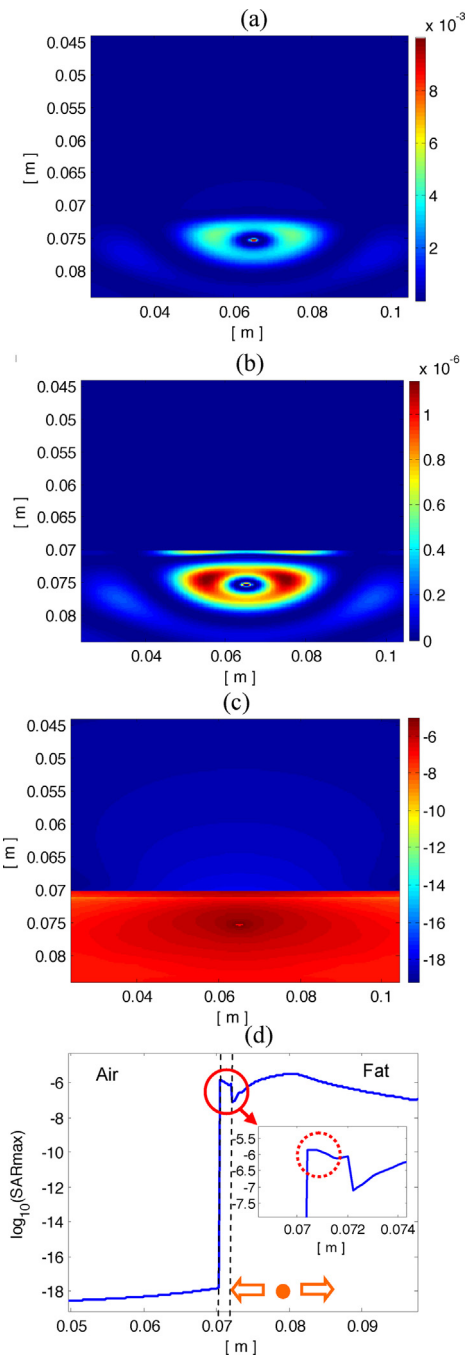

Fig. 5. A contact point source embedded into the skin layer. (a) Instant electric field intensity, (b) instant SAR distribution, (c) logarithmic peak SAR distribution and (d) logarithmic peak SAR distribution on vertical cross-section. Dashed circle in inset plot shows the slight rise as a result of constructive reflection interferences.

Fig. 3 shows the instant electric field intensity distribution in (a), instant SAR distribution in (b), peak SAR distribution in (c) and the logarithmic peak SAR distribution on the vertical cross-section in (d) in the case that a point source is 10 mm above to skin. The distributions are given in a logarithmic scale (to base 10) so as to see the interlayer variation of SAR evidently. Due to reflection from the air–skin interface, a lower EM wave penetration is observed on the air–skin interface (roughly 50 times less as in Fig. 6(a)). However, Fig. 3 (c) and (d) reveals that relatively higher level of SAR is possible in the skin and fat layer because of a large difference between the conductance per density of the skin and the fat tissues ($(\sigma_{eff}/\rho) \cong 59 \times 10^{-4}$ for the skin, $(\sigma_{eff}/\rho) \cong 5 \times 10^{-4}$ for the fat) than the conductance per density of the air tissue $(\sigma_{eff}/\rho) \cong 7 \times 10^{-15}$. Inside the skin and fat layers, attenuation of microwaves is taken place depending on conductance of material. But, a decreasing in SAR level in front of skin layer appears due to the reduction of field intensity (see Fig. 6(a)) associated with destructive reflection interference in Fig. 3(c) and (d). A rise in electric field intensity (see Fig. 6(a)) as a result of constructive reflection interference maintains the SAR level in the thin skin layer.

Fig. 4 illustrates microwave propagation in the case of an embedded point source placed into the skin layer. An noticeable phenomenon was observed in this configuration, that is, the skin

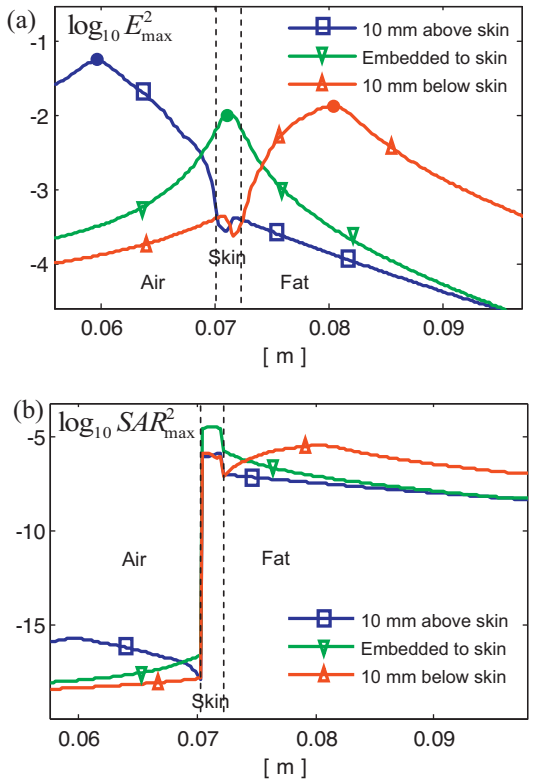

Fig. 6. Comparison of the logarithmic peak electric field intensity (a) and comparison of the logarithmic peak SAR distribution (b) on the vertical cross-section of the skin–fat tissue model for the various point antenna configuration. Dots in green and red indicate locations of the point sources.

layer behaves in a manner similar to wave-guiding effect due to a high reflection coefficients between air–skin and skin–fat interfaces, and hence it transmits the most of the microwave energy inside the skin layer as shown in Fig. 4(a)–(c). This effect leads to a laterally extending high SAR region inside skin layer. This impact on wave propagation possibly results in the microwaves heat much wider skin area comparing to non-contacting and under skin source configurations illustrated in Figs. 3 and 5.

Fig. 5 reveals microwave propagation in the case of an embedded point source placed in a fat layer, where is 10 mm below the skin. The SAR distribution gives a sharp rise on the skin and a sharp fall air–skin interface depending on the conductance per densities of the materials. A signs of lateral wave propagation in a similar manner of wave-guides is apparent in the skin and fat layers in Fig. 5(b) and (c). The increase of SAR in the vicinity of air–skin interface due to constructive reflectance interference is clearly shown inset plot in Fig. 5(d).

The simulations result in Figs. 3–5 are commonly show that there are a sudden SAR drops on the interfaces of the air–skin–fat layers, which severely attenuates a microwave penetration into body. Fig. 6 reveals impacts of various source configurations by showing distribution of the peak electric field intensity and the peak SAR recorded on the vertical cross-section of the skin–fat tissue model during the simulations. Embedding a point source below the skin layer results in a higher energy absorption of the fat tissues. A contact point source embedded into the skin layer provides a higher SAR level up to 2 cm deep into the fat layer than a non-contacting point source above the skin configuration because of a higher electric field intensity penetration. However, the source embedded into the skin and fat configurations spread microwave energy to much wider area inside the layers due to

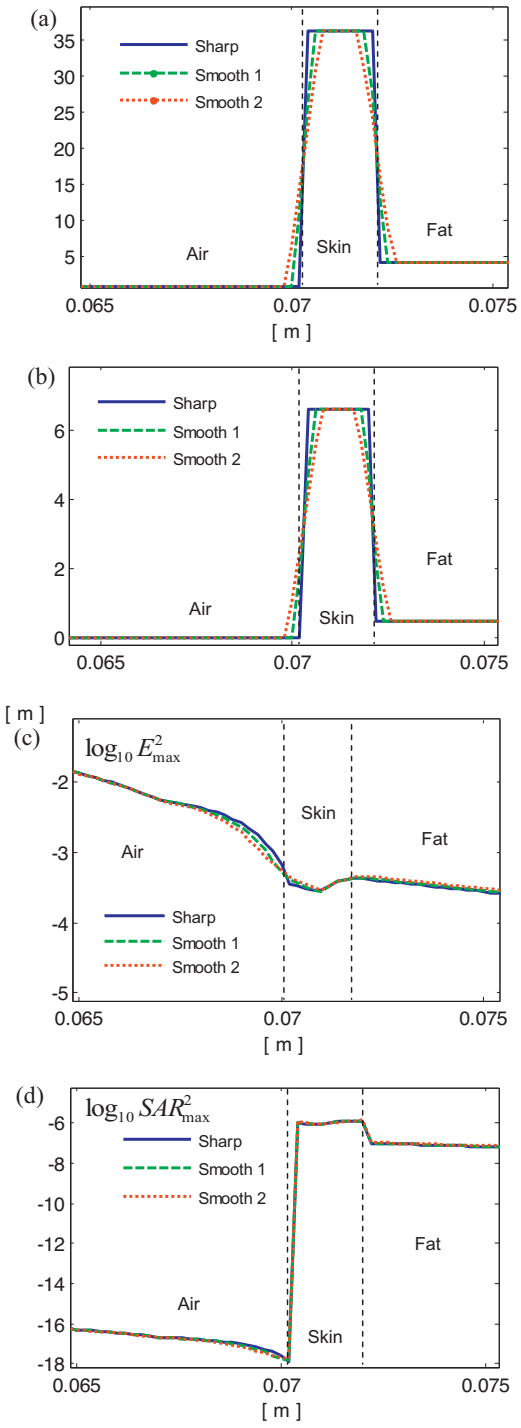

Fig. 7. Comparison of the logarithmic peak electric field intensity (c) and comparison of the logarithmic peak SAR distribution (d) on the vertical cross-section of the skin–fat tissue model for the various smoothing factor of medium parameters (sharp alteration, smooth 1 and smooth 2 alterations of the permittivity (a) and the conductivity (b)).

wave-guiding effect. This effect may not be desirable when an accurate confinement of energy absorption area inside the tissues is needed.

Fig. 7 reveals impacts of gradual alteration of medium parameters between layers. Fig. 7(a) and (b) illustrates sharp and smoothed alterations of medium parameters at layer interfaces. For these parameters alterations, the simulation results, obtained for antenna 10 mm above the skin configuration, are demonstrated in Fig. 7(c)

and (d). The gradual changes of medium parameters between layers result in a minor discrimination in the magnitude of the field intensity and SAR levels. However, the same effects listed in Table 4 and lateral propagation (wave-guide-like effect) inside the skin layer were also observed in the simulation results obtained for the smoothed medium parameters.

4. Conclusions

A multi-layer electrical model of skin–fat tissues were developed and FDTD based simulation of microwave propagation in this tissue model was achieved for various antenna configurations. The simulation results reveal interaction of microwaves in the skin–fat layer up to 2.5 cm depth of fat tissue. Effective physical mechanisms involving in alteration of SAR distribution in a multilayer system with high reflection coefficients are categorized and evaluated by means of FDTD simulation of microwave propagation throughout a skin–fat layer. Sudden SAR changes on the interfaces of air–skin and skin–fat layers were observed in simulation results. This impact principally depends on the large difference in the rate of σ_{eff}/ρ and the impedance mismatches between the layers. The large impedance mismatches result in a high reflection of EM wave from the interfaces of layers and greatly decreases EM wave penetration into the body.

Relatively minor SAR alteration occurs in the vicinity of one side of layer interfaces due to the interference of the reflected and incident waves. Attenuation of the EM wave energy interior of the layers due to electrical losses of the media leads to decreasing of SAR levels depending on distance from interface of layers. However, in a multi-layer system with a high reflection coefficient, this SAR reduction inside layers occurs rather slower than the sharp SAR changing characteristics appearing at the interface of layers as shown in Fig. 5(b).

Skin layer shows a relatively higher conductivity comparing to air and fat layers. This property gains the skin layer a significant reflectivity at 6.8 GHz. Moreover, this property causes spreading the EM energy laterally across the skin layer in a similar manner a waveguide does. This is why; the configuration of an embedded source (applicator) into the fat tissue should be preferred in the medical applications for a condensed energy absorption by the fat layer.

Acknowledgements

The authors would like to thank the anonymous reviewers for their valuable comments and suggestions to improve the quality of the paper.

Appendix A. Derivation of the analytical condition for a sharp SAR alteration concerning with large conductance per mass density discrimination

For a SAR level continuity at the interface of two layers (layer_1 and layer_2), the condition of $(SAR_1/SAR_2) = 1$ in the vicinity of layer interface should be satisfied. Considering Eq. (13) and the transmitted wave energy to layer_2 as $|\vec{E}_2|^2 = (1 - |R|)|\vec{E}_1|^2$, the SAR continuity condition can be arranged as,

$$\frac{\sigma_{eff1}}{\rho_1}\cdot\left(\frac{\sigma_{eff2}}{\rho_2}\right)^{-1} = \frac{|\vec{E}_2|^2}{|\vec{E}_1|^2} = (1 - |R|)$$

A condition for a sharp rising in SAR level at interface of layer_1 and layer_2 ($(SAR_1/SAR_2) \ll 1$) can be deduced as the following,

$$\frac{\sigma_{eff1}}{\rho_1}\cdot\left(\frac{\sigma_{eff2}}{\rho_2}\right)^{-1} \ll (1 - |R|)$$

A condition for a sharp falling in SAR level at interface of layer_1 and layer_2 $(SAR_1/SAR_2) \gg 1$ can be deduced as the following:

$$\frac{\sigma_{eff1}}{\rho_1}\cdot\left(\frac{\sigma_{eff2}}{\rho_2}\right)^{-1} \gg (1 - |R|)$$

References

[1] V.V. Komarov, Formulations of the coupled mathematical models of microwave heating processes, Int. J. Appl. Electromagn. Mech. 36 (2011) 309–316.
[2] J.J. Lagendijk, in: S. Field, C. Franconi (Eds.), Heat Transfer in Tissues: Physics and Technology of Hyperthermia, Nijhoft, Dordrecht, 1987, pp. 517–561.
[3] A. Chichel, J. Skowronek, M. Kubaszewska, M. Kanikowski, Hyperthermia – description of a method and a review of clinical applications, Rep. Pract. Oncol. Radiother. 12 (2007) 267–275.
[4] M.E. Kowalski, J.M. Jin, Model-based optimization of phased arrays for electromagnetic hyperthermia, IEEE Trans. Microw. Theory Tech. 52 (2004) 1964–1977.
[5] Y. Miyazaki, K. Kouno, FDTD analysis of spatial filtering of scattered waves for optical ct of medical diagnosis, in: Progress in Electromagnetics Research Symposium, Beijing, China, 2009, pp. 23–27.
[6] N. Simicevic, D.T. Hayniye, FDTD Simulation of exposure of biological material to electromagnetic nanopulses, Phys. Med. Biol. 50 (2005) 347–360.
[7] M.R. Tofighi, FDTD modeling of biological tissues cole–cole dispersion for 0.5–30 GHz using relaxation time distribution samples—novel and improved implementations, IEEE Trans. Microw. Theory Tech. 57 (2009) 2588–2595.
[8] R. Drezek, A. Dunn, R.R. Kortum, A pulsed finite-difference time-domain (fdtd) method for calculating light scattering from biological cells over broad wavelength ranges, Opt. Express 6 (2000) 147–157.
[9] J.P. Bérenger, A Huygens subgridding for the FDTD method, IEEE Trans. Antenn. Propag. 54 (2006) 3797–3804.
[10] E.K. Wasife, Power density and SAR in multi-layered life tissue at global system mobile (GSM) frequencies, J. Electromagn. Anal. Appl. 3 (2011) 328–332.
[11] B. Tareev, Physics of Dielectric Materials, Mir., Moscow, 1979, pp. 67–174.
[12] G.G. Raju, Dielectrics in electrics fields, in: H.L. Wills (Ed.), Power Engineering Series, vol. 19, Marcel Dekker, New York, 2003.
[13] C. Gabriel, S. Gabriely, E. Corthout, The dielectric properties of biological tissues: I. Literature survey, Phys. Med. Biol. 41 (1996) 2231–2249.
[14] F. Costen, J.P. Bérenger, Extension of the FDTD huygens subgridding to frequency dependent media, Ann. Telecommun. 65 (2010) 211–217.
[15] M. Klemm, G. Troester, EM energy absorption in the human body tissues due to UWB antennas, Prog. Electromagn. Res. PIER 62 (2006) 261–280.
[16] A. Christ, A. Klingenbock, N. Kuster, Energy absorption in layered biological tissues in the near- and far-fields of the antennas of body-mounted devices, in: Proceedings of the XXVIII URSI General Assembly in New Delhi, 2005.
[17] M.E. Chapla, D.P. Nowacek, S.A. Rommel, V.M. Sadler, CT scans and 3d reconstructions of Florida manatee (trichechus manatus latirostris) heads and ear bones, Hearing Res. 228 (2007) 123–135.
[18] A. Taflove, Computational Electrodynamics: The Finite Difference Time Domain Method, Artech House, Boston, 1995.
[19] S. Bri, S. Kassimi, M. Habibi, A. Mamouni, Specific absorption rate (SAR) distribution in the human head at global system mobil (GSM) frequencies, Eur. J. Sci. Res. 49 (2011) 590–600.
[20] M. Mansourabadi, A. Pourkazemi, FDTD hard source and soft source reviews and modifications, Prog. Electromagn. Res. C 3 (2008) 143–160.
[21] K.C. Kao, Dielectric Phenomena in Solids: With Emphasis on Physical Concepts of Electronic Processes, Elsevier Academic Press, San Diego, California, 2004.
[22] R.K. Gangwar, S.P. Singh, D. Kumar, SAR distribution in a bio-medium in close proximity with rectangular dielectric resonator antenna, Progr. Electromagn. Res. B 31 (2011) 157–173.
[23] D. Sullivan, Three-dimensional computer simulation in deep regional hyperthermia using the finite-difference time-domain method, IEEE Trans. Microw. Theory Tech. 38 (1990) 204–211.
[24] E.G. Moros, X. Fan, W.L. Straube, Ultrasound power deposition model for the chest wall, Ultrasound Med. Biol. 25 (1999) 1275–1287.